Journal of Materials Science and Engineering with Advanced Technology
Volume 4, Number 1, 2011, Pages 33-56

METHODOLOGY OF SEMICONDUCTOR SELECTION FOR POLYMER THIN-FILM TRANSISTORS BASED ON CHARGE CARRIER MOBILITY

MARCO ROBERTO CAVALLARI[1], CLEBER ALEXANDRE DE AMORIM[2], GERSON DOS SANTOS[1], SERGIO MERGULHÃO[2], FERNANDO JOSEPETTI FONSECA[1] and ADNEI MELGES DE ANDRADE[3]

[1]Departamento de Engenharia de Sistemas Eletrônicos
Escola Politécnica da Universidade de São Paulo (EPUSP)
Av. Prof. Luciano Gualberto
158 trav. 3, CEP 05508-970
Butantã, São Paulo, SP
Brasil
e-mail: fernando.fonseca@poli.usp.br

[2]Departamento de Física
UFSCar
CP 676, 13565-905
São Carlos, SP
Brasil

[3]Instituto de Eletrotécnica e Energia
USP
Av. Prof. Luciano Gualberto
1289 CEP 05508-970
Butantã, São Paulo, SP
Brasil

Keywords and phrases: PTFT, hole mobility, material selection methodology, MDMO-PPV.

Received July 26, 2011

Abstract

A methodology of material selection for polymer thin-film transistors (PTFT) is important for further improvements in performance and classifying materials for electronics. Charge carrier mobility is believed to be the most important device parameter and was investigated through techniques as time-of-flight (ToF), charge extraction in a linearly increasing voltage (CELIV), current vs. voltage (JxV), and transistor curves. A discussion of the pros and cons of common structures (e.g., planar and vertical) and techniques (e.g., transient and steady-state current measurements) is presented for a well-known semiconductor: poly[2-methoxy-5-(3',7'-dimethyloctyloxy)-1,4-phenylenevinylene] (MDMO-PPV). We demonstrate that the best solution is to have a benchmark bottom gate planar structure and standard characterization conditions (e.g., temperature, light, and humidity) with the proper choice of dielectric and electrodes. Nevertheless, if a rough estimative of the mobility is required, vertical-structured samples for CELIV yields low-cost and fast results.

1. Introduction

Flexible displays and sensors in the field of organic or plastic electronics research have experienced dramatic increase in the current decade, involving many academic and industrial research efforts [34]. Conjugated polymers as poly[2-methoxy-5-(3',7'-dimethyloctyloxy)-1, 4-phenylenevinylene] (MDMO-PPV) can be solution processed and are excellent candidates for low-cost and large-area electronics. MDMO-PPV has been thoroughly studied in solar cells [25, 27, 31], but this polymer can also be used in light-emitting diodes (LED) [1] and transistors for active-matrix organic light emitting diode displays (AMOLED) [35]. Polymer thin-film transistors (PTFT) are very promising devices for the future of flexible electronics thanks to their unique advantages compared to traditional devices, such as low fabrication cost and lightweight [5]. These devices may particularly integrate systems in woven electrotextiles [23] and many branches of sensing (e.g., biomedical diagnosis, food quality monitoring, electronic tongues and noses) [22]. The investigation of new polymeric semiconductors and further development of ambipolar transistors is important for the realization of organic logical circuits, but also of organic light-emitting transistors (OLETs) [29].

Technological advances in PTFTs processing play an important role in the development of organic electronics. Most important device parameters are mobility, on-off modulation, subthreshold slope, threshold voltage, hysteresis, and leakage current. As newly synthesized materials are released continuously, it becomes clear that carrier mobility probably will become the differentiation factor to classify them [21]. Nonetheless, one must take into account that accuracy in mobility measurement may depend on TFT structure, utilized solvents and electrodes, oxide-semiconductor interface, low impurity concentration, and processing techniques [8, 12, 21]. Furthermore, it is not a material but a device parameter, being sensitive to the nanoscale morphology of the organic semiconductor thin film [15]. Commonly employed in charge transport studies, a sandwiched OLED-like structure of films can be prepared for current versus voltage (JxV) measurements and transient current techniques, such as charge extraction in a linearly increasing voltage (CELIV) and time-of-flight (ToF) [4, 17, 37].

In this context, the authors establish a methodology of polymer selection for thin-film transistors based on the active layer mobility characterization by techniques, such as CELIV, ToF, JxV, and transistors. The definition of a set of simple and fast measurements for semiconductor electrical characterization is important for selecting the best suited materials for PTFT-based circuits. Applicability of the herein methodology is demonstrated for MDMO-PPV.

2. Material and Methods

An OLED-like structure was used for JxV, CELIV, and ToF measurements. Indium tin oxide (ITO) electrode over glass (Delta, unpolished, 30-60 Ω / sq.) was patterned on hydrochloric acid (HCl). Prior to polymer deposition, substrates were cleaned on ultrasonic baths of acetone (20 min) and isopropyl alcohol (10 min), with intermediary rinse in ultra-pure water and a final blow dry under nitrogen. MDMO-PPV (Merck KGaA) in (A) 7 and (B) 20mg/ml chloroform solution was agitated for 24 hours, filtered and deposited by spin-coating at (1) 500, (2) 1000 or even (3) 3000rpm for 60 sec. Samples were then heated at 55°C and 0.4mbar during 60 min to eliminate the solvent. Resultant thickness of the films was in the order of a few 100nm and device active area was

9mm^2. A 40nm-thick film of PEDOT:PSS (CLEVIOS P) was processed between ITO electrode and active layer for CELIV and current-voltage measurements. It was deposited in a $0.2\mu\text{m}$-filtered water solution by spin coating at 3000rpm for 30 sec, followed by annealing at 100ºC for 10 min in vacuum. Finally, a 100nm aluminum anode was evaporated by physical vapour deposition (PVD) at 10^{-6} mbar. Device structure and polymer chemical structure are shown in Figure 1(a).

PTFTs were bottom gate and bottom contact devices on a $350\mu\text{m}$-thick heavily doped p-type silicon wafer ($0.020\text{-}0.025\ \Omega.\text{cm}$) acting as substrate and common gate electrode. Prior to dielectric deposition, wafers were chemically cleaned by standard RCA procedure with subsequent etching in diluted HF solution. A 252nm-thick silicon dioxide was grown by dry thermal oxidation. Gold source and drain deposited contacts were 100nm-thick and were obtained by lift-off after electron beam PVD. Channel width/length (W / L) mask values varied from 55 to 220 and L, from 5 to $20\mu\text{m}$. A 100nm-thick MDMO-PPV film was obtained from a 7mg/ml chloroform solution by spin-coating at 3000rpm for 60 sec. TFT structure is shown in Figure 1(b).

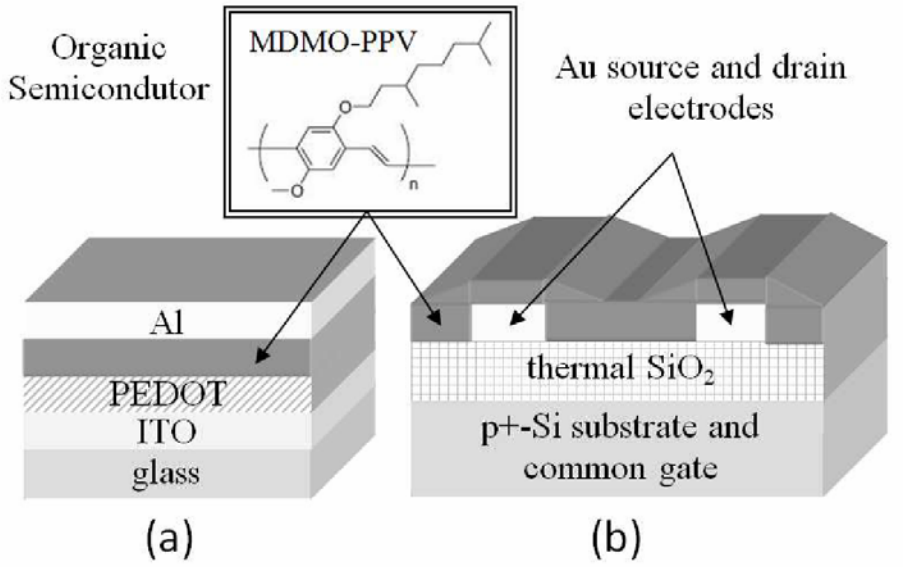

Figure 1. 3-D model of samples for (a) charge transport studies and (b) thin-film transistors. Inset: chemical structure of MDMO-PPV polymer.

Absorption spectrum was obtained with an UV-visible spectrophotometer (Shimadzu, UV-1650 PC) and was necessary for defining the light source for ToF measurements. A 340nm N_2 laser Oriel Instruments Model 79110 was then chosen for these characterizations, together with Tektronix oscilloscope TDS 340A, a Keithley 230 voltage source and a pulse generator Agilent 8013B. Current-voltage measurements (JxV) were performed with a Keithley 237 high-voltage source-measure unit. The oscilloscope and a function generator Agilent 33120A were used for CELIV measurements. When performed in vacuum, it required a Lake Shore 330 temperature controller and a CTI-Cryogenics Model 350C Cryodyne cryocooler. An SR 570 low-noise current preamplifier was placed in series with samples for transient current studies. Transistors were characterized through an Agilent 4156A semiconductor parameter analyzer. TFTs were held at room temperature in darkness and exposed to the atmosphere in a micromanipulator. An Alpha Step 100 profilometer was employed to extract thin-film thickness.

3. Results and Discussion

The following sections deal with common and useful techniques for investigating charge transport in polymeric semiconductors. An analysis of carrier mobility performed in OLED-like samples through ToF, CELIV, and JxV is shown through Subsections 3.1 to 3.3. Finally, results obtained with a benchmark planar thin-film transistor are presented in Subsections 3.4.

3.1. Time-of-flight measurements

Time-of-flight (ToF) is one of the most employed and straightforward technique to extract drift mobility [10]. It consists in the photo-generation of electron-hole pairs by absorption in the semiconducting layer close to a transparent electrode interface, followed by exciton separation under an

applied electric field (E) and the appearance of a transient drift current. While one type of carrier recombines in the irradiated electrode, the oppositely charged carrier drifts through the whole thickness (d) of the sample. Thus, charge carrier mobility (μ) can be calculated from the measured transit time (t_{tr}) by

$$\mu = \frac{d^2}{V \cdot t_{tr}}, \tag{1}$$

where $V = E \cdot d$ is the applied potential.

ToF measured transit times and calculated mobilities are shown in Figure 2 for different thicknesses of the active layer. As charge carriers transit time did not change significantly upon changing the incoming light intensity, it is an indication that the determined transit times were a true measure of photogenerated charge carriers transit time and space charge effects are negligible. For 200nm-thick A1 and B2 samples, mobility is $10^{-5}\mathrm{cm}^2/\mathrm{Vs}$ and 100 times higher than for 400nm, B1 sample. This could be explained by the traps filled within the thin semiconductor film and present in lower concentration. So, charge transport would not be highly dependent on electric field when E approached 1MV/cm. Another hypothesis is that, free carriers are generated all over the thin active layer providing an overestimated mobility. Transit times measured for thinner films (see Figure 2(b)) show almost no variation with respect to electric field, which indicates that carriers are generated everywhere in the semiconductor, diverging from Equation (1). Even if the former explanation was true and real mobility constant, an apparent decrease in mobility with increasing electric field would be expected. This seems to happen to 186 and 240nm films shown in Figure 2(a).

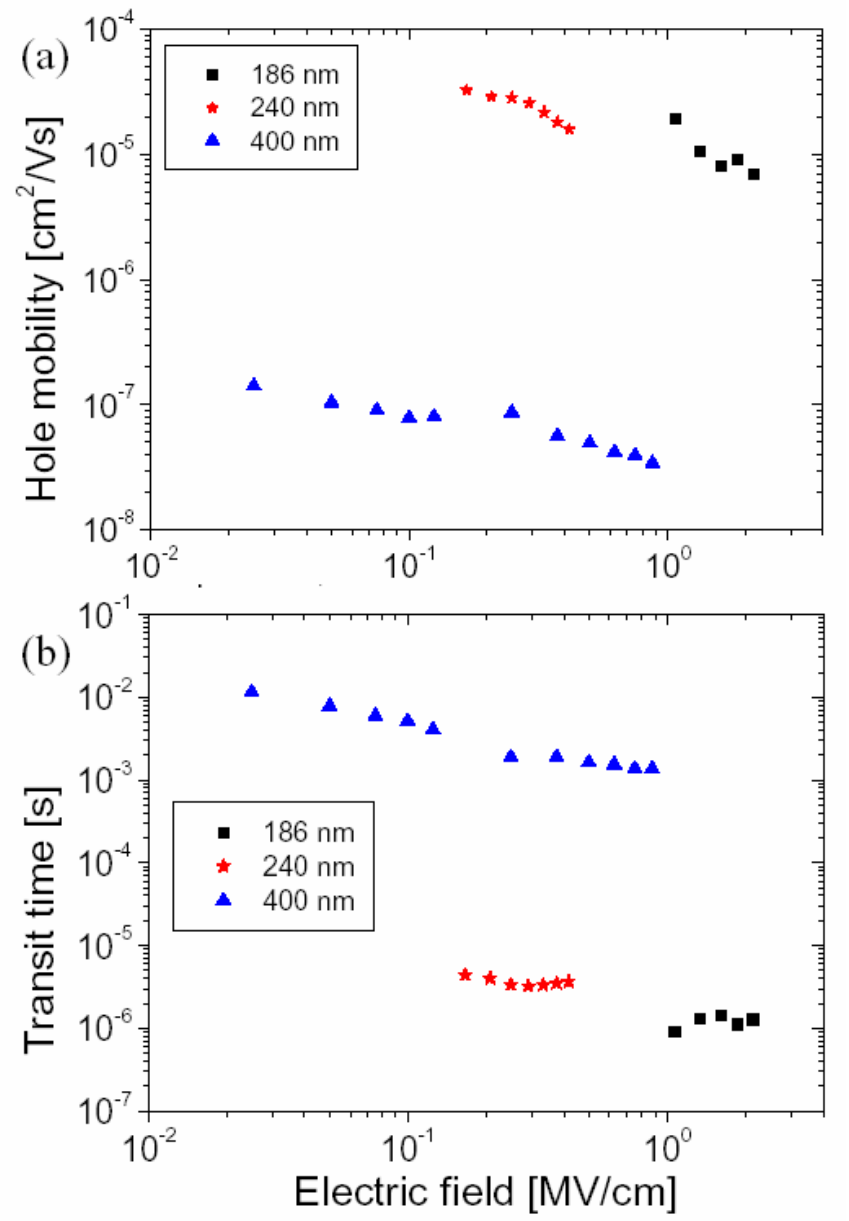

Figure 2. ToF (a) calculated hole mobilities (μ) and (b) measured transit times (t_{tr}) in ITO/MDMO-PPV/Al sandwiched structures with different active layer thicknesses: 186 (squares), 240 (stars), and 400nm (pyramids).

The absorption spectrum of MDMO-PPV is shown in Figure 3(a). As carriers must be generated close to the illuminated electrode/ semiconductor interface within less than 10% deep into the semiconducting layer, the maxima in the absorbance spectrum help in choosing a proper wavelength for optical characterization. Transmittance $(T(\lambda, x))$ given in Figure 3(b) was calculated according to $T(\lambda) = \exp(-\alpha(\lambda)x)$, where $\alpha(\lambda) = (\mathrm{OD}(\lambda)/d)\ln(10)$ is the attenuation coefficient, x the distance from the ITO surface and $\mathrm{OD}(\lambda)$, the optical density. More than the absolute values, it matters the relative values, as T(340nm) > 50% in 186 and 240nm MDMO-PPV films while close to 20% in the thickest one. An observed attenuation factor of $0.003\mathrm{nm}^{-1}$ agrees to Quist et al. [32] results for MDMO-PPV:PCBM bulk heterojunction solar cells. Therefore, thin films under ToF require more complex models, giving away its main quality: drift mobility straightforward estimation.

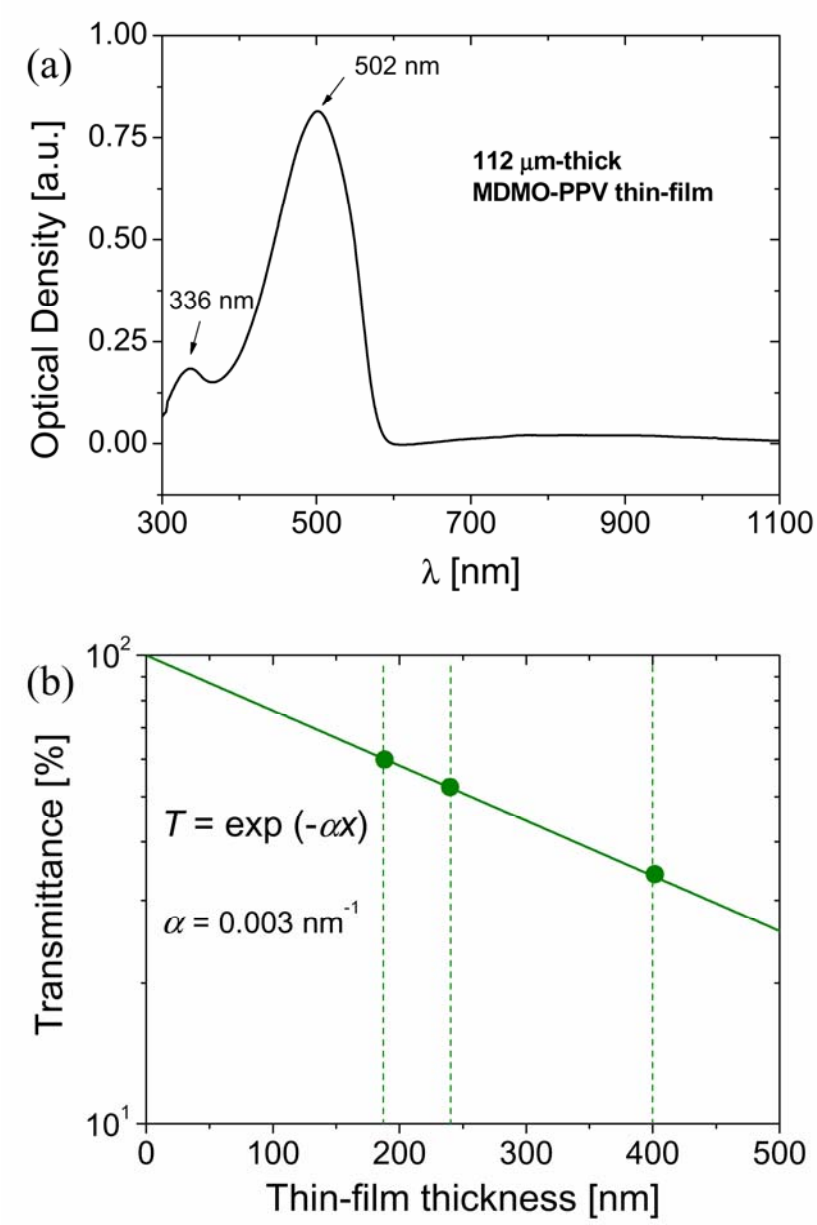

Figure 3. Optical spectra from MDMO-PPV thin-films: (a) optical density (OD) versus wavelength (λ) in a 113nm-thick film and (b) calculated transmittance (*T*) versus penetration depth (*x*).

Differences between samples can also be explained by the chosen spinner speeds or solution concentrations. As largely shown in literature, solution preparation and deposition conditions are highly correlated with the final morphology [16]. As it will be seen in the next sections, a hole mobility in the order of $10^{-8} - 10^{-7} \mathrm{cm}^2 / \mathrm{Vs}$ is expected for this material.

An important condition for the applicability of this technique is that dielectric relaxation time must be longer than charge carrier transit time, $t_\sigma > t_{tr} > 10^{-3}\mathrm{s}$. If this condition is not fulfilled, the equilibrium charge carrier concentration (p_0) can be sufficient to redistribute the electric field inside the sample during a time interval shorter than the small-charge drift time. As a consequence, the apparent charge carrier mobility estimated by the ToF method increases when the electric field decreases, while in reality mobility does not increase. This seems the case of 400nm-thick films and it will be further discussed in Subsection 3.2.

Previous results reported by Tuladhar et al. [37] for polymer thicknesses from 610nm to 1.7μm show dispersive transients (i.e., estimated from the intercept of the asymptotes on a log-log plot) and a Poole-Frenkel-like mobility in the order of $10^{-6} \mathrm{cm}^2 / \mathrm{Vs}$. Even our transients were dispersive, but the observation of a Poole-Frenkel dependence is probably related to adequate thick layers used in the experiment. Mozer et al. [28] did not find any mobility variation by changing the sample thickness, nonetheless the active layer ranged from 0.32 to 2.3μm.

3.2. Charge extraction in a linearly increasing voltage measurements

CELIV technique, proposed initially by Juška et al. in 1999 [18], appears as an alternative for ToF on the frame of highly-conductive materials characterization such as microcrystalline silicon (μc - Si:H). It has already been demonstrated useful for studying π-conjugated polymers with exponential distribution of traps in energy such as poly(3-hexylthiophene) (P3HT) [17]. One of its merits lies in the possibility to study charge transport in nanometric films, resulting in less material

waste and allowing to study films as processed in an industrial device. A disadvantage lies in the impossibility to analyze minority carriers within the same sample. Hole mobility (μ) and film conductivity (σ) for MDMO-PPV are shown in Figure 4.

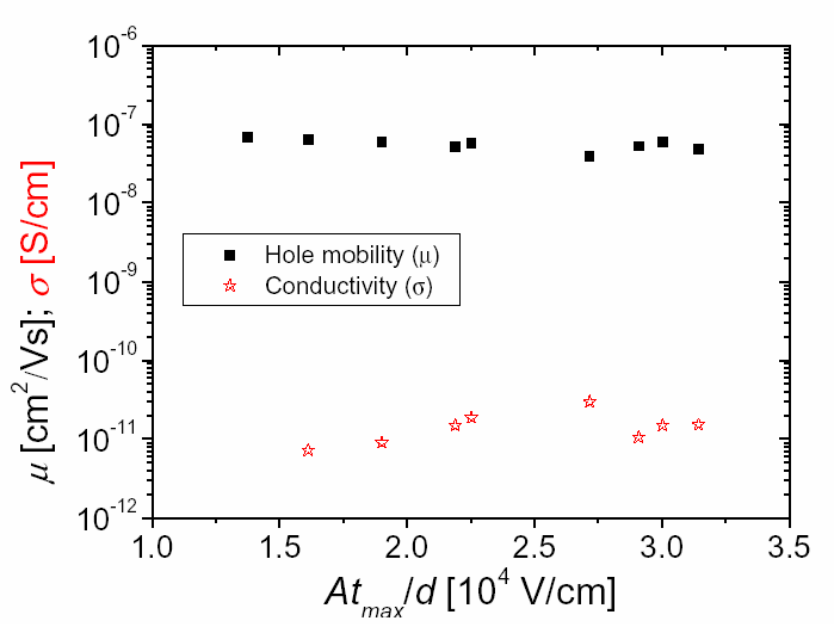

Figure 4. CELIV calculated hole mobility μ (filled squares) and conductivity σ (empty stars) in function of the electric field for a ITO/PEDOT:PSS/MDMO-PPV(400nm, B1)/Al sample.

Formulae applied are

$$\mu = \frac{2d^2}{2At_{\max}^2[1 + 0.36(\Delta J / J(0))]}; \tag{2}$$

and

$$\sigma = \frac{3\varepsilon_r\varepsilon_0\Delta J}{2t_{\max}J(0)}, \tag{3}$$

where A is the voltage rise speed, $t_{\max}$ is the time to maximum $\Delta J = J_{\max} - J(0)$ of the extraction peak, $J(0)$ is the displacement current of the capacitance, ε_r is the material relative dielectric permittivity (2.1 for MDMO-PPV [26]), and ε_0 is the vacuum permittivity.

Mobilities are approximately constant and equal to $6 \times 10^{-8} \mathrm{cm}^2 / \mathrm{Vs}$ at low electric fields and agree well with results by ToF in 400nm-thick films. As mobility is not varying with the electric field, the condition $t_\sigma > t_{tr}$ seems not to be respected, leading to an apparent decrease of ToF mobility. Relaxation time $-t_\sigma = \varepsilon_r \varepsilon_0 / \sigma$ [18]– from 1×10^{-2} to $1 \times 10^{-1} \mathrm{s}$ is higher than t_{tr} in Figure 2(b). Juška et al. [19] demonstrated this effect in details for regioregular poly(3-octyl thiophene) (P3OT). Dennler et al. [11] used a variation of the technique called photo-CELIV for studying MDMO-PPV:PCBM bulk heterojunction solar cells. The thickness of the device was comprised between 150 and 250nm, resulting in $\mu \sim 2 \times 10^{-6} \mathrm{cm}^2 / \mathrm{Vs}$ for 100% MDMO-PPV films. The discrepancy with these earlier results might originate in different processing conditions, but also in an overestimation of the real mobility by Dennler et al. [11].

3.3. Current-voltage measurements

Depending on the adopted model for charge transport in a semiconductor, carrier mobility can be extracted from steady state JxV curves. Most used models are divided into limited by either injection or bulk mechanisms [4, 20]. Thermionic emission, Richardson-Schottky and Fowler-Nordheim, all of them injection models, are chosen for rectifying contacts and do not provide any information on traps distribution or charge carrier mobility. Bulk charge transport requires the presence of hardly achievable Ohmic injecting contacts. Most commonly used bulk-limited transport models are Ohm's law and space-charge limited currents (SCLC). The latter group will be detailed in the following:

Ohmic conduction is predominant for low levels of injection, i.e., when the density of thermally generated carriers p_0 inside the specimen is larger than the density of injected carriers. This is characterized by a linear relationship between JxV given by

$$J = q\mu p_0 \frac{V}{d}, \tag{4}$$

where q is the elementary charge. Considering a trap-free semiconductor, when injected carriers are able to travel all the way between the electrodes and their concentration overcomes p_0, the onset of the SCLC takes place. The current expression is given by Mott-Gurney law

$$J = \frac{9}{8}\varepsilon_r\varepsilon_0\mu\frac{V^2}{d^3}. \tag{5}$$

In the presence of shallow traps (i.e., a localized energetic level between hole quasi-Fermi level and valence band upper limit), mobility is modulated by a θ factor in (5). If traps are confined in a single level with concentration H, the trap filling limited voltage V_{TFL} is given by

$$V_{TFL} = \frac{qHd^2}{2\varepsilon_r\varepsilon_0}. \tag{6}$$

A space-charge-limited current with shallow trap-limited intermediary regime was observed for a 108nm-thick A3 MDMO-PPV film (see Figure 5(a)). Hole mobility was calculated from (5), being equal to 3.9×10^{-11} and $2.7\times10^{-7}\text{cm}^2/\text{Vs}$ for lower and higher voltage regimes, respectively. Modulation factor θ is 9.5×10^{-6} for a trap concentration H of $1.7\times10^{16}\text{cm}^{-3}$, calculated from (6). A PEDOT:PSS thin-film was necessary for attaining Ohmic contacts and improving interface quality with the organic semiconductor. Blom et al. [3] showed that hole conduction in MDMO-PPV OLEDs is space-charge limited with $\mu = 5\times10^{-7}\text{cm}^2/\text{Vs}$. MDMO-PPV thicknesses of 130, 300, and 700nm between ITO and Au electrodes were studied assuming $\varepsilon_r = 3$. At high

electric fields ($> 0.3\text{MV}/\text{cm}$), they observed a gradual deviation from (5) with exponential increase of the mobility ($\alpha \exp[\gamma(E)^{1/2}]$).

In the presence of an exponential distribution of traps in energy $(E) - h(E) = (H/kT_c)\exp(E/kT_c)$–, Mott-Gurney law becomes

$$J = e^{1-l}\mu N_v\left(\frac{2l+1}{l+1}\right)^{l+1}\left(\frac{l}{l+1}\frac{\varepsilon_r\varepsilon_0}{H}\right)^{l}\frac{V^{l+1}}{d^{2l+1}}, \tag{7}$$

where N_v is the effective density of states in the valence band (here estimated as $1.1\times10^{18}\text{cm}^{-3}$) and l is related to the characteristic constant (T_c) of the traps distribution through $l = T_c/T$, being T the temperature. By setting (4) equal to (7), the applied voltage V_Ω required for the transition between regimes is

$$V_\Omega = \frac{qd^2H}{\varepsilon_r\varepsilon_0}\left(\frac{p_0}{N_v}\right)^{1/l}\left(\frac{l+1}{l}\right)\left(\frac{l+1}{2l+1}\right)^{(l+1)/l}. \tag{8}$$

When all traps are filled up, a transition from trapped to trap-free SCLC will take place. By setting (5) equal to (7), the required voltage V_{TFL} becomes

$$V_{TFL} = \frac{qd^2}{\varepsilon_r\varepsilon_0}\left[\frac{9}{8}\frac{H^l}{N_v}\left(\frac{l+1}{l}\right)^{l}\left(\frac{l+1}{2l+1}\right)^{l+1}\right]^{1/(l-1)}. \tag{9}$$

The two latter transitions were observed for a 190nm-thick A2 MDMO-PPV film (see Figure 5(b)). Trap-free SCLC for higher voltages is characterized by $\mu = 2.3\times10^{-8}\text{cm}^2/\text{Vs}$. In linear regime (i.e., $\text{J}\,\alpha\,\text{V}$), by using the trap-free mobility, it is possible to obtain the concentration of thermally generated carriers (p_0), that is, $1.0\times10^{13}\text{cm}^{-3}$. By applying (7) to (9) in the $\text{J}\,\alpha\,\text{V}^{4.8}$ regime, we obtain $l = 3.8$, $T_c = 1144\,\text{K}$, $p_0 = 8.7\times10^{12}\text{cm}^{-3}$, $H = 1.1\times10^{17}\text{cm}^{-3}$, and $\mu = 2.8\times10^{-8}\text{cm}^2/\text{Vs}$. Hole mobility and thermally generated carrier concentration calculated in the three different regimes agree perfectly.

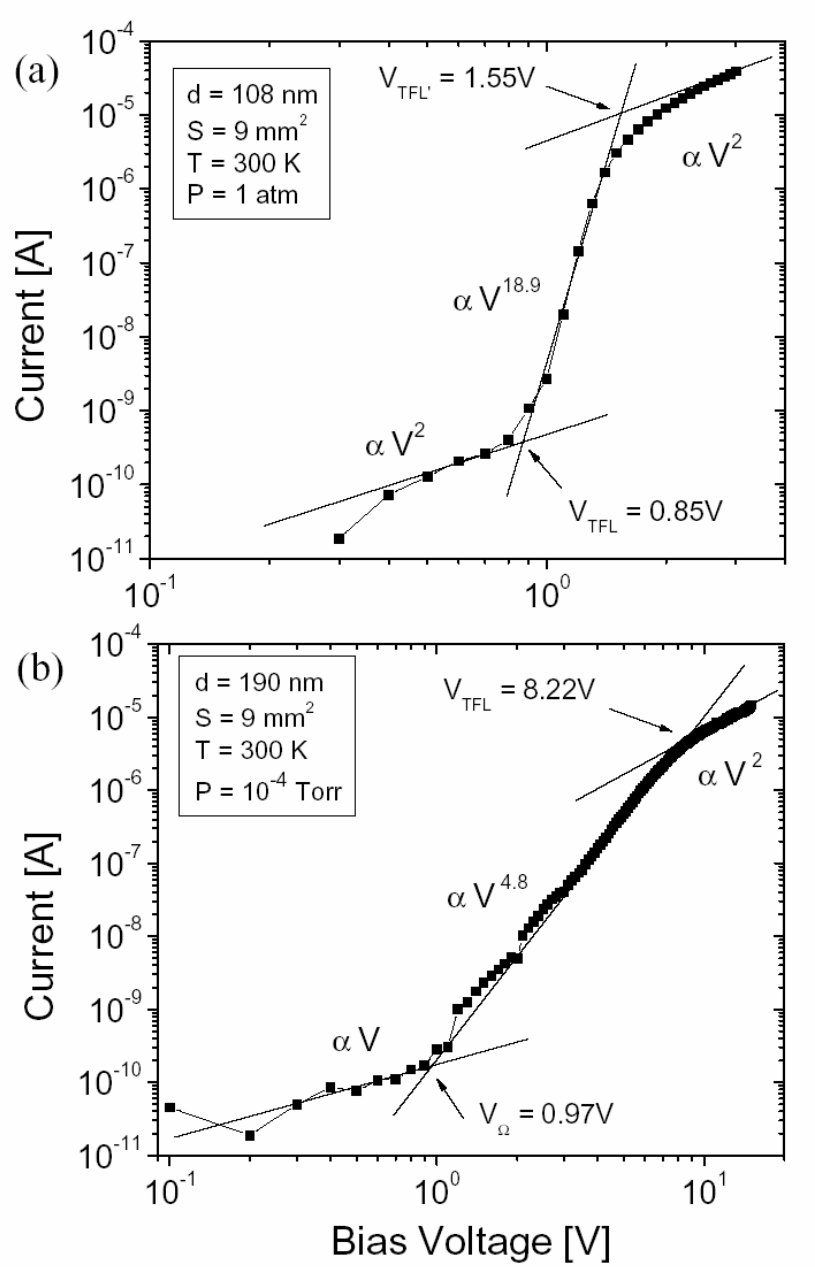

Figure 5. Space-charge limited regimes in ITO/PEDOT:PSS/MDMO-PPV/Al samples: (a) one single shallow trap energetic level and (b) exponential distribution of traps with Ohmic conduction for lower voltages and trap-free SCLC for higher voltages.

Similar to already hypothesized in Subsection 3.1, depending on processing conditions, different behaviours are expected to appear in JxV characteristics. Trapping in deep energetic levels in the semiconductor impacts on curves repeatability and can make it difficult to investigate the electrical properties of new polymeric semiconductors. For instance, nanomorphology in van der Waals crystals depends on film preparation, such as solvent molecular formula and evaporation time, substrate temperature and deposition method [2, 14]. Oxygen trapping during processing and characterization can also affect the charge transport regimes observed from JxV curves [24]. Thus, a more desirable panorama would demands film deposition conditions identical to the actual transistor. As transient current techniques usually require submicrometer films (e.g., > 500nm), this is not generally the case. Considering as an approximation $E = V / d$ and constant, theoretical transit time obtained through (1) is 2.8×10^{-4} and 1.9×10^{-3}s for 108 and 190nm-thick films, respectively. These values agree well with what is obtained by ToF for 400nm-thick films (see Figure 3(b)).

3.4. Polymer thin-film transistors

The choice of a well-known TFT structure for studying the organic semiconductor is important at early stages of device development. For this purpose, thin-film transistors on highly doped silicon substrates covered by a high quality thermally grown SiO_2 as gate dielectric layer were used. Differently from inorganic monocrystalline counterparts, electrical transport in polymeric semiconductors is inherently anisotropic at the molecular scale as charges are delocalized within the conjugation length along the backbone of a polymer, being the rate-limiting step of transport the interchain hopping of charges. In an organic transistor, charge carrier mobility is commonly assumed dependent on the overdrive voltage (i.e., the difference between gate voltage V_{GS} and threshold voltage V_T) through

$$\mu = k(V_{GS} - V_T)^{\gamma}, \tag{10}$$

where k contains information on film morphology, being mainly related to the ease of intersite hopping, and γ is related to the broadness of an exponential DOS by $\gamma = 2(T_c / T - 1)$. One possible explanation lies in the variable-range hopping model proposed by Vissenberg and Matters [38], where carriers contribute to current flow only when they are excited to a so-called transport energy level. At higher carrier concentration, the average starting energy is closer to the transport energy, which reduces the activation energy and therefore enhances mobility. Drain current (I_D) in linear regime becomes

$$I_D = C_{ox} \frac{W}{L} k(V_G - V_T)^{\gamma+1}.V_D, \tag{11}$$

where C_{ox} is the dielectric capacitance per area, W is the channel width, L is the channel length, and V_D is the drain voltage. In saturation regime, the saturation current becomes

$$I_D = C_{ox} \frac{W}{L} k \frac{1}{\gamma + 2} (V_G - V_T)^{\gamma+2}. \tag{12}$$

Applying the methodology for parameter extraction from I_D versus V_{GS} curves presented in [30] and partially exposed above, we obtained the results shown in Table 1. For high-mobility organic crystals $(\mu > 0.1\text{cm}^2 / \text{Vs})$, where channel resistance can be much lower than contact resistance, a model including series resistance effects is given in [30]. Mobilities calculated at $V_{GS} = -40\text{V}$ for different channel lengths agree well and reach 0.9×10^{-5} and $2.2 \times 10^{-5}\text{cm}^2 / \text{Vs}$ for linear and saturation regimes, respectively. Similar results were obtained by Todescato et al. [36] for a wet cleaning of SiO_2 without fluoridric acid, where $\mu_h = 2.5 \times 10^{-5}\text{cm}^2 / \text{Vs}$ and $V_T = -8.7\text{V}$. MDMO-PPV was deposited from a chlorobenzene solution on a bottom gate top contact structure and channel length was higher than 100μm.

Table 1. TFT parameters extracted from linear and saturation regimes. For all the devices, $C_{ox} = 13.7 \times 10^{-9}\,\mathrm{F/cm^2}$ and $W = 1.1\mathrm{mm}$

Regime	**L** [μm]	**k** $[10^{-7}\mathrm{cm^2/V^{\alpha}s}]$	$\mathbf{V_T}$ [V]	$\boldsymbol{\gamma}$	$\mathbf{T_c}$ [K]	$\boldsymbol{\mu_{max}}(V_{GS} = -40\mathrm{V})$ $[10^{-5}\mathrm{cm^2/Vs}]$	$\mathbf{V_T'}$ [V]	**μ'** $[10^{-5}\mathrm{cm^2/Vs}]$
Linear $V_{DS} = -5\mathrm{V}$	4	5.6	8.1	0.58	390	0.52	– 2.3	0.70
	9	12.3	6.1	0.41	360	0.59	3.8	0.57
	19	3.0	9.6	0.88	430	0.93	1.8	0.87
Saturation $V_{DS} = -40\mathrm{V}$	4	5.1	12	0.93	440	2.0	– 1.6	2.5
	9	5.2	7.4	0.93	440	1.9	– 5.0	2.4
	19	4.1	11	1.0	450	2.1	– 3.5	2.8

Considering a simpler model with constant mobility calculated from $dI_D^{1/2}/dV_G$ (see μ' in Table 1), we observe that μ' approaches μ at $V_{GS} = -40\text{V}$, providing no information on the mobility dependence with gate voltage. Calculated threshold voltages (V_T') differ between linear and saturation regimes and are usually more negative than values estimated from more precise models (see V_T in Table 1). Both fitting methods in saturation regime are shown along with experimental data in Figure 6(a). It is clear that a varying mobility fits much better at lower voltages, as already remarked by Shaked et al. [33]. For voltages close to zero, there are three main sources of error: leakage current through the dielectric (in our case, less than 1nA), residual carrier concentration in the channel when the device is turned off and films composed of two or more phases with different DOS [33].

A plot of the mobility in function of the overdrive voltage (V_{OV}) is shown in Figure 6(b). For lower gate voltages and consequently lower charge concentration in the channel, a higher similarity with the values presented in the previous sections is observed. Anyway, as demonstrated by Tanase et al. [35], differences of three orders of magnitude in mobility are expected between TFT and LED-like samples from the same semiconductor. Hole mobilities attained are $4.7 \times 10^{-4}\text{cm}^2/\text{Vs}$ at $V_{GS} = -19\text{V}$ for a channel width and length of 2 500μm and 10μm, respectively, and MDMO-PPV was deposited from a toluene solution. Calculated characteristic temperatures (T_c) also differ from charge transport studies. As demonstrated elsewhere by Cavallari et al., not all differences are related to processing conditions: dielectric-related properties (e.g., V_T, C_{ox}, and surface) must be the same while testing more than one polymer [13]. Among many updates to be brought to IEEE standard for testing organic transistor [6], the authors remark also serious resistance (e.g., a set of W or L mask values) and environment conditions.

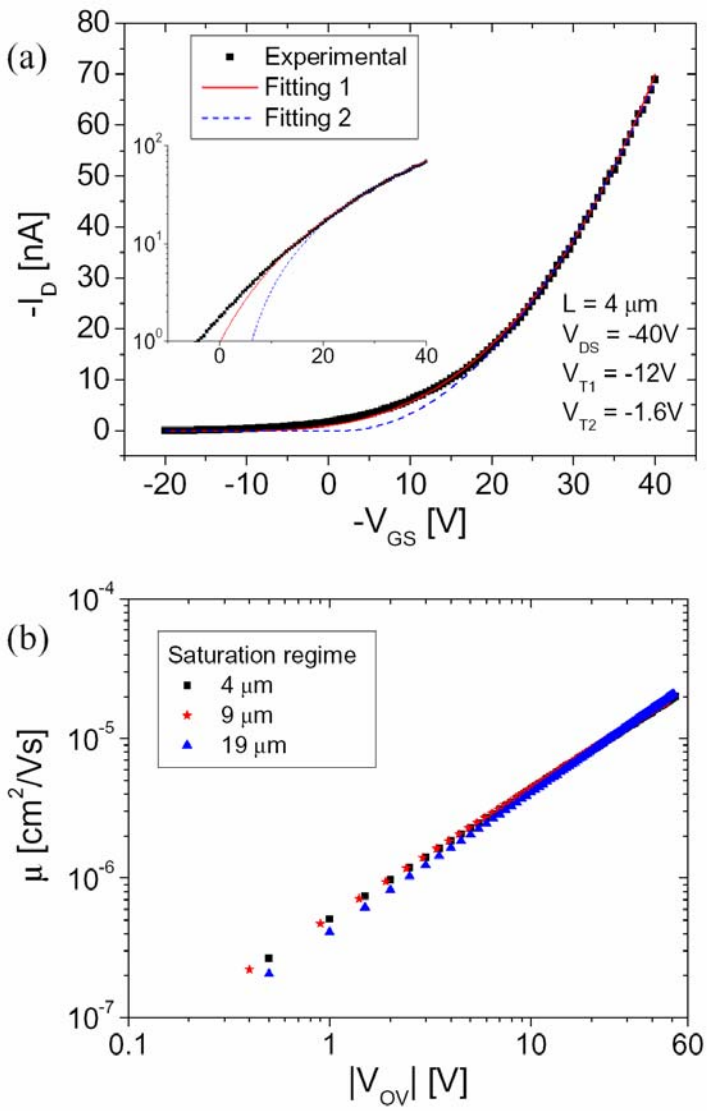

Figure 6. MDMO-PPV TFT characterization results: (a) I_D versus V_{GS} experimental data for L = 4μm in saturation regime. Fitting method 1 considers a gate voltage-dependent mobility (μ = $f(V_{GS})$), while fitting method 2 uses a constant μ. Inset: same plot of I_D versus V_{GS}, but in logarithmic scale; (b) mobility dependence on the overdrive voltage for different channel lengths: 4 (squares), 9 (stars), and 19μm (pyramids).

Taking into account the horizontal electric field (E_{ll}) due to V_{DS}, we observe that μ doubles from -5 to -40V. Investigating new materials requires not only fixing the dielectric properties, but also the ratio V_{DS}/L. The detailed analysis of μ dependence on E_{ll} for these transistors was already published elsewhere [7].

Finally, V_T should ideally approach zero, otherwise, it is an indication of defects occurring at the polymer-oxide interface, arising from charged defects in the oxide or the polymer. In this case, a proper self-assembled monolayer or a polymeric buffer thin film can be applied prior to semiconductor deposition [36]. Cavallari et al. [7] demonstrated hole mobilities of $1\times10^{-4}\text{cm}^2/\text{Vs}$ and almost no hysteresis for hexamethy-ldisilazane (HMDS) surface treatment. The authors believe a more hydrophobic surface with lower $-$OH concentration is responsible for the better results.

4. Conclusion

Knowledge obtained from studying charge transport varies according to the chosen technique. Time-of-flight (ToF) requires thicker films than the ones employed in the actual devices, but it is the most straightforward for mobility calculation. Charge extraction in a linearly increasing voltage (CELIV) does not need expensive lasers and has already been successfully applied to organic thin films (~100nm) – avoiding unnecessary material waste –, but it demands more than one sample with different electrode Fermi levels for studying both types of carrier. Current-voltage measurements offer a lot of information on the mobility dependence on electric field and traps distribution of states, but it needs Ohmic contact to achieve bulk-limited charge transport. Due to the high quantity of available models, the analysis can become slow and costly. These three techniques have in common low carrier concentration and a mobility two to three orders of magnitude lower than in a TFT of the same semiconductor. Therefore, the best solution is to set a

benchmark thin-film transistor structure and standard characterization conditions (e.g., temperature, light, and humidity). This work considered a silicon substrate covered with HMDS-treated thermal SiO_2 and Au electrodes as the best TFT structure for studying the PPV derivative.

When studying a new material, even with a TFT structure a good alignment between the Fermi level of the metal electrode and the highest occupied molecular orbital, HOMO (lowest unoccupied molecular orbital, LUMO), for a *p*-type (*n*-type) organic semiconductor is necessary. An initial study on HOMO/LUMO levels can be done with cyclic voltammetry and UV-visible absorption spectroscopy [9]. A previous study of solution preparation and thin film morphology is necessary for controlling roughness, thickness, and wettability.

Acknowledgement

The authors would like to thank the Brazilian agencies FAPESP (07/06064-0; 09/05589-7) and CNPq (MCT/CT-INFO 17/2009, 14230 2/2010-4) for financial support. Special thanks to the cleanroom and Microwaves Laboratory staffs, Carlos A. R. Santos, Katia F. Albertin, Roberto K. Onmori (Laboratório de Microeletrônica, EPUSP) for devices fabrication, Luiz F. R. Pereira (Universidade de Aveiro, Portugal), Luca Fumagalli, Dario Natali and Marco Sampietro (Politecnico di Milano, Italy) for fruitful discussions.

References

[1] A. L. Alvarez, B. Arredondo, B. Romero, X. Quintana, A. Gutierrez-Llorente, R. Mallavia and J. M. Oton, IEEE Trans. Elect. Dev. 55 (2008), 674.

[2] A. C. Arias, J. D. MacKenzie, R. Stevenson, J. M. Halls, M. Inbasekaran, E. P. Woo, D. Richards and R. H. Friend, Macromolecules 34 (2001), 6005.

[3] P. W. M. Blom and M. J. M. de Jong, IEEE J. Sel. Top. Quantum Electron. 4 (1998), 105.

[4] D. Braun, J. Pol. Sci. Part B: Pol. Phys. 41 (2003), 2622.

[5] A. L. Briseno, S. C. B. Mannsfeld, M. M. Ling, S. Liu, R. J. Tseng, C. Reese, M. E. Roberts, Y. Yang, F. Wudl and Z. Bao, Nature 444 (2006), 913.

[6] M. R. Cavallari, K. F. Albertin, G. Santos, C. A. S. Ramos, I. Pereyra, F. J. Fonseca and A. M. Andrade, J. Int. Circ. Syst. 5 (2010), 116.

[7] M. R. Cavallari, K. F. Albertin, G. Santos, C. A. S. Ramos, I. Pereyra, F. J. Fonseca and A. M. Andrade, ECS Trans. 31 (2010), 425.

[8] M. L. Chabinyc and A. Salleo, Chem. Mater. 16 (2004), 4509.

[9] D. Chirvase, Z. Chiguvare, M. Knipper, J. Parisi, V. Dyakonov and J. C. Hummelen, Synth. Met. 138 (2003), 299.

[10] Z. Deng, S. T. Lee, D. P. Webb, Y. C. Chan and W. A. Gambling, Synth. Met. 107 (1999), 107.

[11] G. Dennler, N. S. Sariciftci, A. J. Mozer, A. Pivrikas, R. Österbacka and G. Juška, Org. Electron. 7 (2006), 229.

[12] C. D. Dimitrakopoulos and D. J. Mascaro, IBM J. Res. Dev. 45 (2001), 11.

[13] IEEE Standards 1620 (2004), 1.

[14] A. Gadisa, M. Svensson, M. R. Andersson and O. Inganäs, Appl. Phys. Lett. 84 (2004), 1609.

[15] H. Hoppe, M. Niggemann, C. Winder, J. Kraut, R. Hiesgh, A. Hinsch, D. Meissner and N. S. Sariciftci, Adv. Funct. Mater. 14 (2004), 1005.

[16] H. Hoppe and N. S. Sariciftci, J. Mater. Chem. 16 (2006), 45.

[17] G. Juška, K. Arlauskas, M. Viliūnas, K. Genevičius, R. Österbacka and H. Stubb, Phys. Rev. B 62 (2000), R16235.

[18] G. Juška, K. Genevičius, M. Viliūnas, K. Arlauskas, H. Stuchlíková, A. Fejfar and J. Kočka, J. Non-Crystal. Sol. 266-269 (2000), 331.

[19] G. Juška, K. Genevičius, K. Arlauskas, R. Österbacka and H. Stubb, Phys. Rev. B 65 (2002), 233208.

[20] M. Lampert, Phys. Rev. 103 (1956), 1648.

[21] A. Lodha and R. Singh, IEEE Trans. Semic. Manuf. 14 (2001), 281.

[22] J. T. Mabeck and G. G. Malliaras, Anal. Bioanal. Chem. 384 (2005), 343.

[23] M. Maccioni, E. Orgiu, P. Cosseddu, S. Locci and A. Bonfiglio, Appl. Phys. Lett. 89 (2006), 143515.

[24] G. G. Malliaras, Y. Shen, D. H. Dunlap, H. Murata and Z. H. Kafafi, Appl. Phys. Lett. 79 (2001), 2582.

[25] M. M. Mandoc, W. Veurman, L. J. A. Koster, M. M. Koetse, J. Sweelssen, B. de Boer and P. W. M. Blom, J. Appl. Phys. 101 (2007), 104512.

[26] H. C. F. Martens, H. B. Brom and P. W. M. Blom, Phys. Rev. B 60 (1999), R8489.

[27] A. C. Mayer, S. R. Scully, B. E. Hardin, M. W. Rowell and M. D. McGehee, Mater. Today 10 (2007), 28.

[28] A. J. Mozer, P. Denk, M. C. Scharber, H. Neugebauer and N. S. Sariciftci, J. Phys. Chem. B 108 (2004), 5235.

[29] M. Muccini, Nat. Mater. 5 (2006), 605.

[30] D. Natali, L. Fumagalli and M. Sampietro, J. Appl. Phys. 101 (2007), 014501.

[31] A. Pivrikas, N. S. Sariciftci, G. Juška and R. Österbacka, Prog. Photovolt: Res. Appl. 15 (2007), 677.

[32] P. A. C. Quist, T. Martens, J. V. Manca, T. J. Savenije and L. D. A. Siebbeles, Solar Energy Materials & Solar Cells 90 (2006), 362.

[33] S. Shaked, S. Tal, Y. Roichman, A. Razin, S. Xiao, Y. Eichen and N. Tessler, Adv. Mater. 15 (2003), 913.

[34] Th. B. Singh and N. S. Sariciftci, Annu. Rev. Mater. Res. 36 (2006), 199.

[35] C. Tanase, E. J. Meijer, P. W. M. Blom and D. M. de Leeuw, Phys. Rev. Lett. 91 (2003), 216601.

[36] F. Todescato, R. Capelli, F. Dinelli, M. Murgia, N. Camaioni, M. Yang, R. Bozio and M. Muccini, J. Phys. Chem. B 112 (2008), 10130.

[37] S. M. Tuladhar, D. Poplavskyy, S. A. Choulis, J. R. Durrant, D. D. C. Bradley and J. Nelson, Adv. Funct. Mater. 15 (2005), 1171.

[38] M. C. J. M. Vissenberg and M. Matters, Phys. Rev. B 57 (1998), 12964.

■